25th ABCM International Congress of Mechanical Engineering
October 20-25, 2019, Uberlândia, MG, Brazil

COB-2019-0854
PHYSICAL MATHEMATICAL AND COMPUTATIONAL MODELING OF THE TWO-DIMENSIONAL FLOW OVER A HEATED POROUS SQUARE CYLINDER

Ítalo Augusto Magalhães de Ávila
Gabriel Machado dos Santos
Hélio Ribeiro Neto
Aristeu da Silveira Neto
Federal University of Uberlândia, Av. João Naves de Ávila 2121, Campus Santa Mônica. Uberlândia, MG, Brazil, CEP 38400-902.
italo.ufuracing@gmail.com, gabriel.msantos@ufu.br, heliorine@hotmail.com, aristeus@ufu.br

Abstract. *In this paper the authors present the physical, mathematical and computational modeling of the laminar flow through a heated square cylinder composed of a porous medium. The modeling equations are solved in a two-dimensional fixed Eulerian and Cartesian domain through the finite-difference method. Streamlines and temperature iso-surfaces are presented for different values of porosity and permeability. The results obtained with the in-house developed code are in accord with those encountered in literature.*

Keywords: *computational fluid dynamics, numerical simulation, porous media, backward-facing step*

1. INTRODUCTION

The dynamic and thermal phenomena associated with flows through porous media have been a subject of great interest of scientists and engineers because of its wide application in materials, mechanical, chemical and biomedical engineering. The modeling of more realistic applications require the solution of fluid only and porous regions jointly, interaction present in mechanisms such as catalytic converters, thermal energy exchangers and gas turbines.

The mechanics of flows through porous media is traditionally modeled according to the empirical Darcy-Forchheimer model, which describes the main effects of the porous media through the conciliation of inertial and viscous effects (linear and non-linear corrections). The energy transport, on its turn, is based on the volumetric-average of the properties of fluid and solid phases, as presented by Vafai (2005). This methodology can be found in the works of Lauriat and Prasad (1989), Goyeau and Songbe (1996) and Al-Amiri (2000).

Although the geometry of the porous structure presented in this paper is canonical, its interaction with the fluid can offer significant insights of features such as vortex shedding, flow separation, wake formation and thermal distribution. Information of great interest for the design of cooling towers and grain cooling systems, for instance. Some effort was invested in similar analysis, as observed in the works of Chen *et al.* (2008), Dhinakaran and Ponmozhi (2011) and Mahdhaoui *et al.* (2017).

An in-house code was developed and simulations were conducted in order to evaluate the joint influence of porosity and permeability over the flow and the temperature field. The modeling equations are solved in a two-dimensional fixed Eulerian and Cartesian domain through the finite-difference method. The results are analyzed and compared with those available in the literature.

2. PHYSICAL AND DIFFERENTIAL MODELING

For the modeling of the flow through a heated porous square cylinder, it is possible to model the fluid as Newtonian and the flow as incompressible. The solid phase physical properties are modeled as homogeneous and isotropic through the domain. A graphic representation of the domain and of the boundary conditions is presented at Fig. (1), in which D represents the edge of the porous square and L represents a given dimension of the channel ($L_{top} = L_{bot} = L_{left} = 15D$ and $L_{right} = 50D$).

For the differential modeling of fluid mechanics, the application of Reynolds transport theorem, Newton's second law and energy balance in a differential volume, provide the relations required to describe the movement of the fluid and evaluate the energy transport and transformations. The first, when employed to the analysis of the mass flux through a control volume (REV), provides the continuity equation, which ensures that the mass balance will be respected. The linear momentum equations (or Navier-Stokes equations) are obtained from Newton's second law, that presents the relation

between the acceleration perceived by the system and the external forces acting upon it. Finally, the solution of the temperature field is possible through the thermal energy balance in a control volume (differential energy equation).

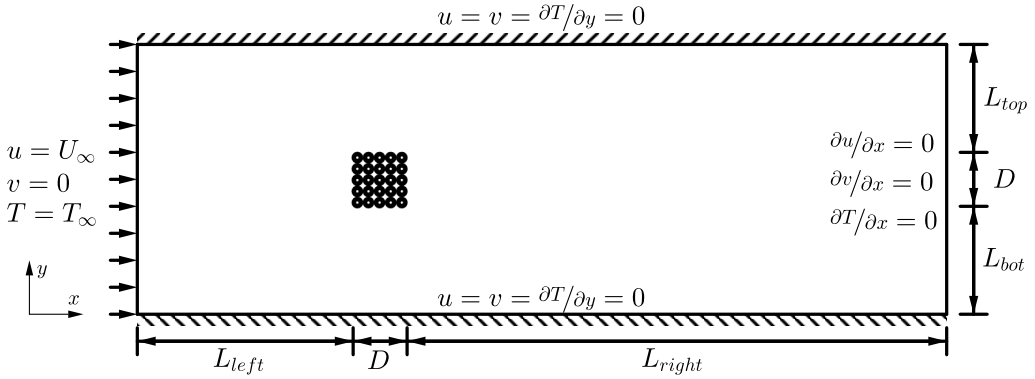

Figure 1: Graphic representation of the boundary conditions.

For the modeling of flows through isotropic porous media, Darcy-Forchheimer empirical model proposes the addition of a source therm for the linear momentum equation, described as follows.

$$-\boldsymbol{\nabla} P_{pore} = \frac{\mu \mathbf{V}}{K} + \frac{F\rho|\mathbf{V}|\mathbf{V}}{\sqrt{K}}, \tag{1}$$

where $\boldsymbol{\nabla} P_{pore}$ is the pressure drop due to the interaction with the porous medium, μ the fluid dynamic viscosity, K the permeability, $\mathbf{V}$ the velocity vector, ρ the specific mass of the fluid and F the Forchheimer coefficient (function of porosity and microscopic solid geometry).

For the modeling of the thermal phenomena, the thermal energy equation must account for the conduction, by both fluid and solid phases, and the advection, which occurs only for the fluid phase. Physical properties of the porous medium may be estimated by their volumetric average, function of the porosity (ratio between fluid and total volume in the system).

$$(\rho C)_m = \varepsilon (\rho C)_f + (1-\varepsilon)(\rho C)_s, \tag{2}$$

$$k_m = \varepsilon k_f + (1-\varepsilon) k_s, \tag{3}$$

where the subscripts f, s and m refer to the properties of fluid, solid and porous medium, respectively. The specific thermal capacity is given by C, the thermal conductivity coefficient by k, and the porosity by ε.

The continuity, linear momentum and energy equations for the flow through an isotropic porous media are presented bellow:

$$\boldsymbol{\nabla} \cdot \mathbf{V} = 0, \tag{4}$$

$$\frac{1}{\varepsilon}\frac{\partial \mathbf{V}}{\partial t} + \frac{1}{\varepsilon^2}(\mathbf{V}\cdot\boldsymbol{\nabla})\mathbf{V} = -\frac{1}{\rho}\boldsymbol{\nabla} p - \mathbf{g}\beta(T - T_o) + \frac{\nu}{\varepsilon}\boldsymbol{\nabla}^2\mathbf{V} - \frac{\nu}{K}\mathbf{V} - \frac{F|\mathbf{V}|\mathbf{V}}{\sqrt{K}}, \tag{5}$$

$$(\rho C)_m \frac{\partial T}{\partial t} + (\rho C)_f \mathbf{V}\cdot\boldsymbol{\nabla} T = k_m \boldsymbol{\nabla}^2 T + \phi, \tag{6}$$

where p represents the pressure, $\mathbf{g}$ the gravity field, β the thermal expansion coefficient, ν the kinematic viscosity (ratio of the viscosity to the specific mass), ϕ the viscous transformation function, T the volume averaged temperature (fluid and solid phases jointly) and T_o the reference temperature. With this set of equations the incompressible flows of newtonian fluids through an homogeneous porous medium in transient regime are modeled.

For the modeling of the flow through non-porous regions, the Darcy-Forchheimer correction and the thermal tortuosity effects are suppressed, and the Eq.(5) and (6) are reduced to the classical Navier-Stokes equations and the differential thermal energy equation, presented bellow:

$$\frac{\partial \mathbf{V}}{\partial t} + (\mathbf{V}\cdot\boldsymbol{\nabla})\mathbf{V} = -\frac{1}{\rho}\boldsymbol{\nabla} p - \mathbf{g}\beta(T - T_o) + \nu\boldsymbol{\nabla}^2\mathbf{V}, \tag{7}$$

$$(\rho C)_f \frac{\partial T}{\partial t} + (\rho C)_f \mathbf{V}\cdot\boldsymbol{\nabla} T = k_f \boldsymbol{\nabla}^2 T + \phi. \tag{8}$$

The non-isothermal constant inlet velocity flow over an immersed body is usually characterized by the Reynolds number ($Re = \rho V D/\mu$) and the Prandtl number ($Pr = \nu/\alpha$). Considering that the body consists of a porous medium, parameters such as the conductivity ratio ($\lambda = k_f/k_m$), Darcy number ($Da = K/L^2$) and porosity (ε) must also be accounted for. The symbol α represents the thermal diffusivity.

3. NUMERICAL MODEL

With the physical and differential models defined, a numerical model can be used to obtain an approximate solution to this problem. The domain is discretized evenly and Taylor's expansion is used to the approximation of both first (CDS or Central Difference Scheme) and second order derivatives. For a function in a two-dimensional space, the domain may be written as follows:

$$\mathcal{M} = \{(t^N, x_I, y_J);\ t^N = N\Delta t,\ x_I = I\Delta x,\ y_J = J\Delta y,\ N = 0, 1, \ldots, K,\ I = 0, 1, \ldots, L,\ J = 0, 1, \ldots, M\} \quad (9)$$

The equations presented previously can only be applied to a continuous domain and must be rewritten. The modified value for the horizontal and vertical velocity components ($\hat{u}$ and $\hat{v}$, respectively) are estimated from the following equations:

$$\hat{u}_{I,J} = -\left(\varepsilon\,\delta_p + \delta_f\right)\Delta t\beta\left[\frac{T^N_{I-1,J} + T^N_{I,J}}{2T_o} - 1\right] g_x - \left(\varepsilon\,\delta_p + \delta_f\right)\frac{\Delta t}{\rho}\,\frac{p^N_{I,J} - p^N_{I-1,J}}{\Delta x} -$$
$$\frac{\Delta t}{\varepsilon\,\delta_p + \delta_f}\,u^N_{I,J}\,\frac{u^N_{I+1,J} - u^N_{I-1,J}}{2\Delta x} - \frac{\Delta t}{\varepsilon\,\delta_p + \delta_f}\,v^N_{I,J}\,\frac{u^N_{I,J+1} - u^N_{I,J-1}}{2\Delta x} - \varepsilon\,\delta_p\frac{F|V^N_{I,J}|u^N_{I,J}}{\sqrt{K}} +$$
$$\frac{\Delta t\,\mu}{\rho}\,\frac{u^N_{I+1,J} - 2u^N_{I,J} + u^N_{I-1,J}}{\Delta x^2} + \frac{\Delta t\,\mu}{\rho}\,\frac{u^N_{I,J+1} - 2u^N_{I,J} + u^N_{I,J-1}}{\Delta y^2} - \varepsilon\,\delta_p\frac{\mu}{\rho K}u^N_{I,J} + u^N_{I,J}, \quad (10)$$

$$\hat{v}_{I,J} = -\left(\varepsilon\,\delta_p + \delta_f\right)\Delta t\beta\left[\frac{T^N_{I,J-1} + T^N_{I,J}}{2T_o} - 1\right] g_y - \left(\varepsilon\,\delta_p + \delta_f\right)\frac{\Delta t}{\rho}\,\frac{p^N_{I,J} - p^N_{I,J-1}}{\Delta y} -$$
$$\frac{\Delta t}{\varepsilon\,\delta_p + \delta_f}\,v^N_{I,J}\,\frac{v^N_{I,J+1} - v^N_{I,J-1}}{2\Delta y} - \frac{\Delta t}{\varepsilon\,\delta_p + \delta_f}\,u^N_{I,J}\,\frac{v^N_{I+1,J} - v^N_{I-1,J}}{2\Delta x} - \varepsilon\,\delta_p\frac{F|V^N_{I,J}|v^N_{I,J}}{\sqrt{K}} +$$
$$\frac{\Delta t\,\mu}{\rho}\,\frac{v^N_{I+1,J} - 2v^N_{I,J} + v^N_{I-1,J}}{\Delta x^2} + \frac{\Delta t\,\mu}{\rho}\,\frac{v^N_{I,J+1} - 2v^N_{I,J} + v^N_{I,J-1}}{\Delta y^2} - \varepsilon\,\delta_p\frac{\mu}{\rho K}v^N_{I,J} + v^N_{I,J}, \quad (11)$$

where δ_p and δ_f are Kronecker delta functions used to mark porous and non-porous regions, respectively.

The correction for the pressure (p^o) is obtained from the continuity equation, as indicated in Eq.(12), and the value of the velocity components must be corrected from its modified value through this correction. The pressure field is logged at each time step as presented in Eq.(14).

$$\boldsymbol{\nabla}^2 p^o = \boldsymbol{\nabla}\cdot\mathbf{V} \approx \frac{\hat{u}_{I+1,J} - \hat{u}_{I,J}}{\Delta x} + \frac{\hat{v}_{I,J+1} - \hat{v}_{I,J}}{\Delta y}, \quad (12)$$

$$u^{N+1}_{I,J} = \hat{u}_{I,J} - \frac{p^o_{I,J} - p^o_{I-1,J}}{\Delta x}, \quad (13)$$

$$p_{I,J} = p_{I,J} + p^o_{I,J}. \quad (14)$$

The energy equation, in its turn, can be rewritten as indicated bellow. In Eq. (15), the parameters $\check{u}$ and $\check{v}$ represent the interpolated velocity components.

$$T^{N+1}_{I,J} = \Delta t(\delta_f\alpha_f + \delta_p\alpha_m)\left[\frac{T^N_{I+1,J} - 2T^N_{I,J} + T^N_{I-1,J}}{\Delta x^2} + \frac{T^N_{I,J+1} - 2T^N_{I,J} + T^N_{I,J-1}}{\Delta y^2}\right] -$$
$$\frac{\Delta t(\rho C)_f}{\delta_f(\rho C)_f + \delta_p(\rho C)_m}\left[\check{u}^N_{I,J}\,\frac{T^N_{I+1,J} - T^N_{I-1,J}}{2\Delta x} - \check{v}^N_{I,J}\,\frac{T^N_{I,J+1} - T^N_{I,J-1}}{2\Delta x}\right] + T^N_{I,J} + \Phi^N_{I,J}. \quad (15)$$

4. VALIDATION

The validation of the developed computational model is conducted through the comparison between the results obtained and the ones encountered in the literature for low values of the Darcy number. It is also convenient to compare the results of the flow over a porous cylinder with the one over its solid counterpart, since flows through porous structures with low values of the Darcy number should present similar characteristics of those over a solid, non-permeable, body.

Simulations are conducted for $\varepsilon = 10^{-2}$ and $Da = 10^{-6}$, an uniform spatial increment of approximately $6.67\ mm$ and a fix time step of $10^{-4}\ s$. The results are compared to the works of Anirudh and Dhinarakan (2018), which models the flow over a porous square cylinder, and Sharma and Eswaran (2004), which presents results for the flow over its solid equivalent.

Streamlines for the flows over a porous square cylinder and over a solid one are presented at Fig.(2). It is possible to observe that the porous matrix exerts a significant resistance to the fluid's movement, both through its borders and in its interior, fact that justifies the aforementioned comparison. At Tab.(1), the average drag coefficients and the recirculating lengths are presented. The results obtained are in accord to those found in the literature. The employed spatial and time increments proved sufficient to capture with appreciable accuracy the linear momentum transport phenomena.

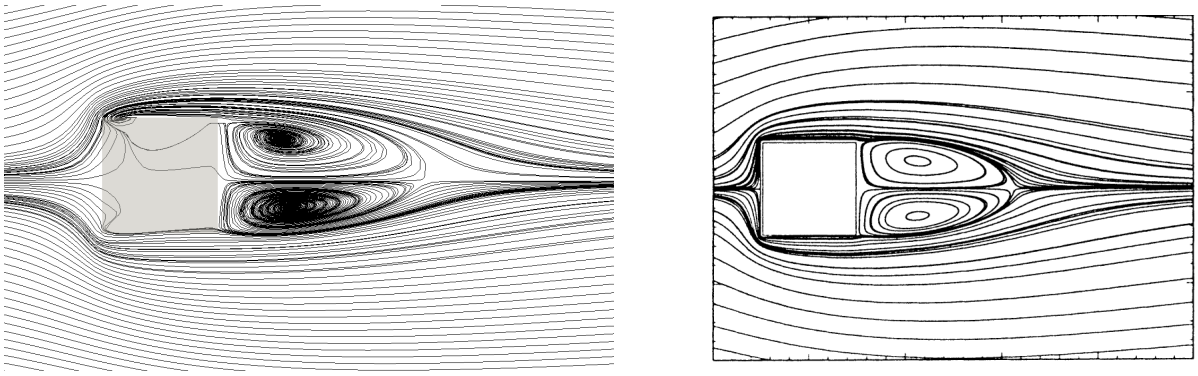

(a) (b)

Figure 2: Streamlines for the flow with $Re = 30$ over: (a) a porous square cylinder ($\varepsilon = 10^{-2}$,$Da = 10^{-6}$) and (b) a solid square cylinder(Breuer *et al.*, 2000).

Table 1: Drag coefficient (C_d) and recirculating length (L_{rec}) for $Re = 30$ and $Re = 100$.

Re		C_d	L_{rec}
30	Present work	–	2.0840
	Anirudh and Dhinarakan (2018)	–	2.1140
	Sharma and Eswaran (2004)	–	2.1100
100	Present work	1.4954	–
	Anirudh and Dhinarakan (2018)	1.5120	–
	Sharma and Eswaran (2004)	1.4947	–

It is also convenient to compare the vortex shedding frequency between solid and porous geometries. For this purpose, a probe is fixed at a distance of $10D$ downstream the obstacle, and, for each time step, the vertical velocity component is stored. The signal is then treated through the Fourier transform and its composing frequencies are evaluated in the form of the dimensionless Strouhal number (St). The data acquisition period was defined as $t = [20, 60]$ seconds. The results obtained in the present work for a porous square cylinder, with $\varepsilon = 10^{-2}$ and $Da = 10^{-6}$, and the ones encountered in the literature for its solid counterpart are presented at Tab.(2).

Table 2: Strouhal number for the flow over a square cylinder with $Re = 100$.

	St
Present work	0.1537
Robichaux *et al.* (1999)	0.1540
Sharma and Eswaran (2004)	0.1488
Sahu *et al.* (2009)	0.1486

5. RESULTS

In this section, the results obtained with the developed computational model are presented. Simulations were conducted for $Re = 100$, $Pr = 0.71$, $\lambda = 1$ and different values of porosity and permeability (Darcy's number). Spatial and time increments are defined as approximately $6.67\ mm$ and $10^{-4}\ s$, same values used for the validation case. A thermal energy transformation function, of $5 \cdot 10^9\ W/m^2$, is imposed to the solid fraction of the porous medium in order to evaluate the thermal energy transport and transformation phenomena.

The simulations are conducted for a null gravitational field, so that the temperature field does not introduces distortions to the linear momentum transport phenomena. The thermal energy, in this case, can be used as a tracer for the fluid that comes in contact with the porous structure. Thus, despite the diffusive mechanisms, undesirable for the purposes of a tracer, it is possible, through the temperature field, to visualize the trajectory of a particle that comes into contact with the porous medium.

Streamlines and temperature iso-surfaces are presented at Figs.(3) and (4), respectively. In such figures, it is possible to observe the formation of Von Karman structures downstream the obstacle. Such formations are product of instabilities that, for virtual experimentation, are of numeric nature. The set of equations that models the fluid mechanics constitutes an unstable dynamic system that, for certain proportions between inertial and viscous effects, can reach a turbulent regime. It should be noted that these structures do not characterize turbulence, but simply display the unstable nature of the system.

It is interesting to point that, in experimental studies, the instabilities, and the Von Karman structures, are also present, but they are of a random nature and can be associated to misalignments, geometric imperfections of the body or the channel, vibrations transported by structures, among many other factors.

The vortices are associated to low pressure regions, which promote the oscillations observed in the drag and lift coefficients (C_d and C_l, respectively), presented at Fig.(6). Such coefficients are function of forces due to viscous effects, which can be calculated directly at the interface, and due to the pressure field, which must be extrapolated (not coincident with the interface). The increase in the medium's permeability should result in lower drag coefficients and lower amplitudes for the lift coefficient. This is not observed, however, in this paper's results. It is not possible to say if this is a physical response, justified by the formation of pressure gradients inside the porous structure, or if it is a flaw in the methodology employed in the calculation of the forces acting on the interface. In future studies, greater clarity on the question can probably be achieved if the calculation of the coefficients is conducted through the Reynolds Transport Theorem.

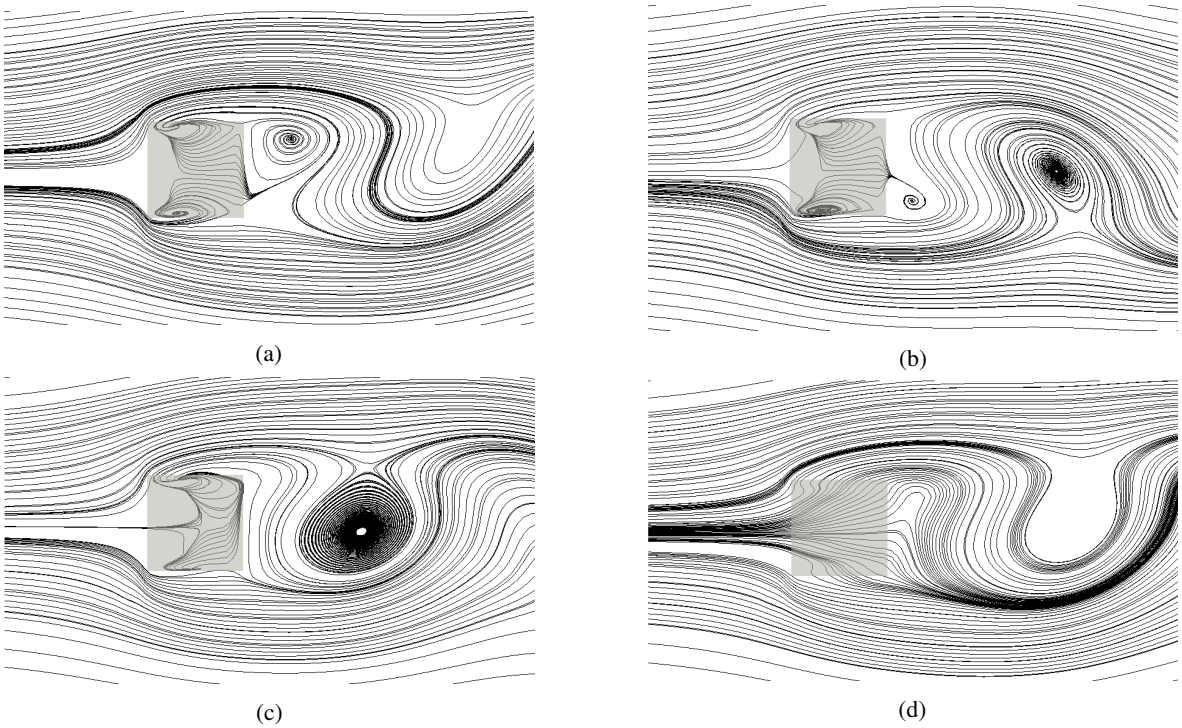

Figure 3: Streamlines for the flow over a porous square cylinder at $t = 30\ s$ with $Re = 10^2$: (a) $\varepsilon = 10^{-2}$, $Da = 1 \cdot 10^{-6}$, (b) $\varepsilon = 5 \cdot 10^{-2}$, $Da = 1 \cdot 10^{-5}$, (c) $\varepsilon = 10^{-1}$, $Da = 1 \cdot 10^{-4}$, (d) $\varepsilon = 1,5 \cdot 10^{-1}$, $Da = 1 \cdot 10^{-3}$.

Strouhal numbers for the different configurations of the case are presented in Fig.(5), and the higher amplitude frequencies are compiled in Tab.(3). From these, it is possible to observe that an increase in the values of porosity and permeability results in a slight elongation of the vortices and, consequently, a lower shedding frequency. The justification for this correlation lies on the fact that, increments over these parameters are associated to a reduction in the medium's

resistance to the transport of fluid and, consequently, of linear momentum through the porous matrix. It is expected that the amplification of instabilities will be hampered and the vortex shedding will be delayed until, finally, a combination of porosity and permeability will completely inhibit their formation.

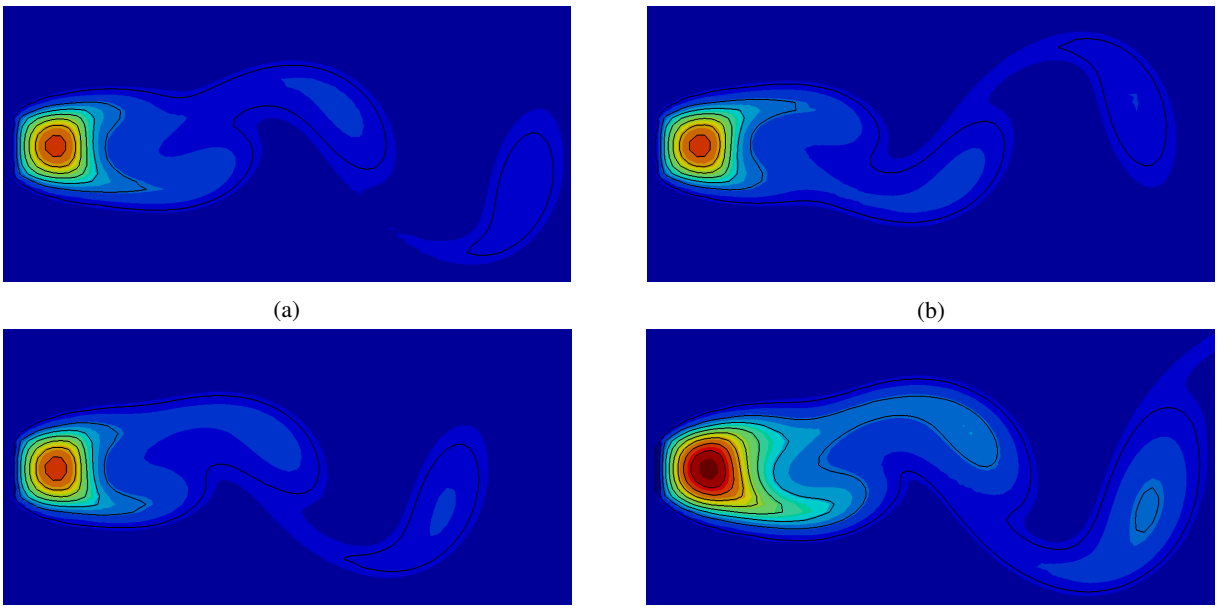

(a) (b) (c) (d)

Figure 4: Temperature iso-surfaces for the flow over a porous square cylinder at $t = 30\ s$ with $Re = 10^2$: (a) $\varepsilon = 10^{-2}$, $Da = 1 \cdot 10^{-6}$, (b) $\varepsilon = 5 \cdot 10^{-2}$, $Da = 1 \cdot 10^{-5}$, (c) $\varepsilon = 10^{-1}$, $Da = 1 \cdot 10^{-4}$, (d) $\varepsilon = 1,5 \cdot 10^{-1}$, $Da = 1 \cdot 10^{-3}$.

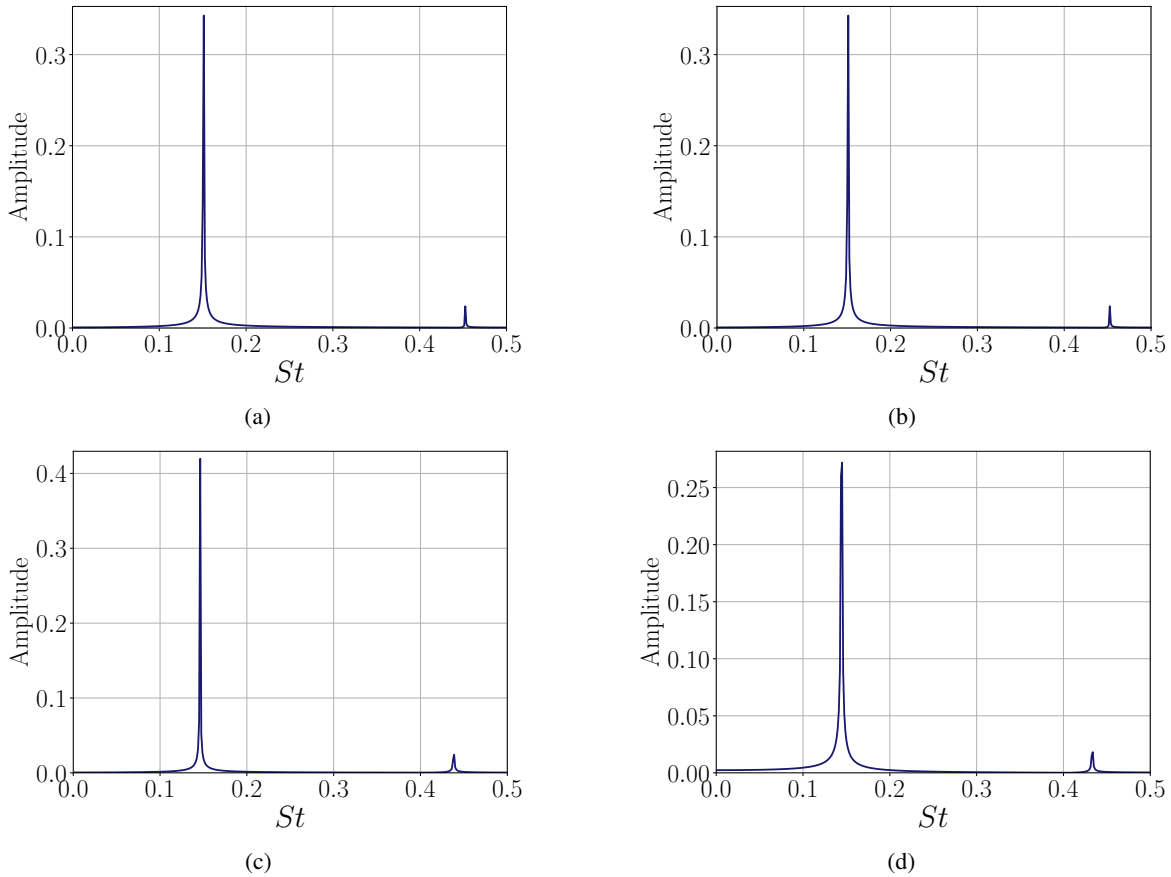

(a) (b) (c) (d)

Figure 5: Strouhal numbers for the flow over a porous square cylinder with $Re = 10^2$: (a) $\varepsilon = 10^{-2}$, $Da = 1 \cdot 10^{-6}$, (b) $\varepsilon = 5 \cdot 10^{-2}$, $Da = 1 \cdot 10^{-5}$, (c) $\varepsilon = 10^{-1}$, $Da = 1 \cdot 10^{-4}$, (d) $\varepsilon = 1,5 \cdot 10^{-1}$, $Da = 1 \cdot 10^{-3}$.

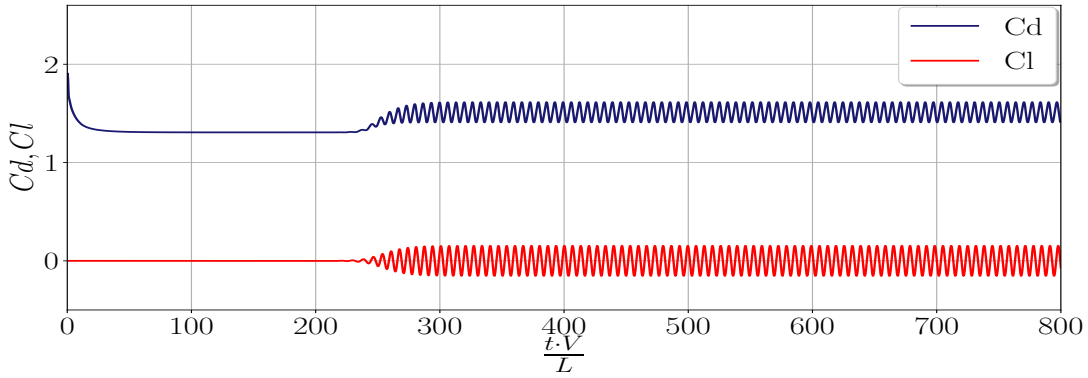

(a)

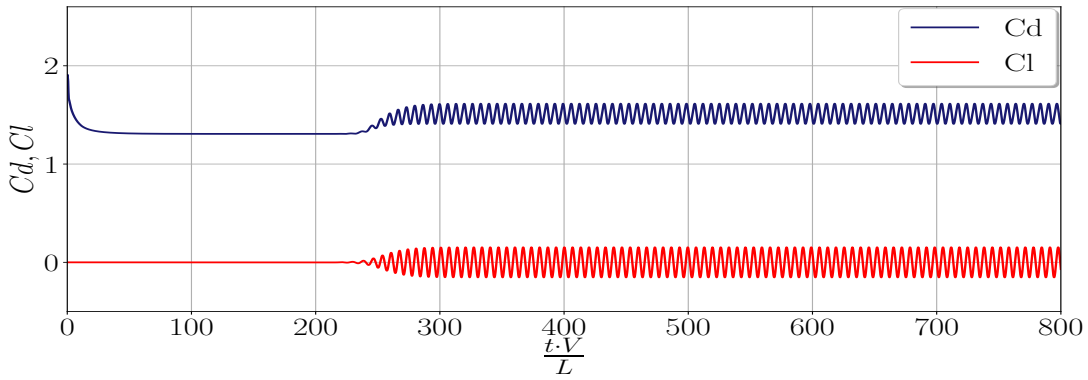

(b)

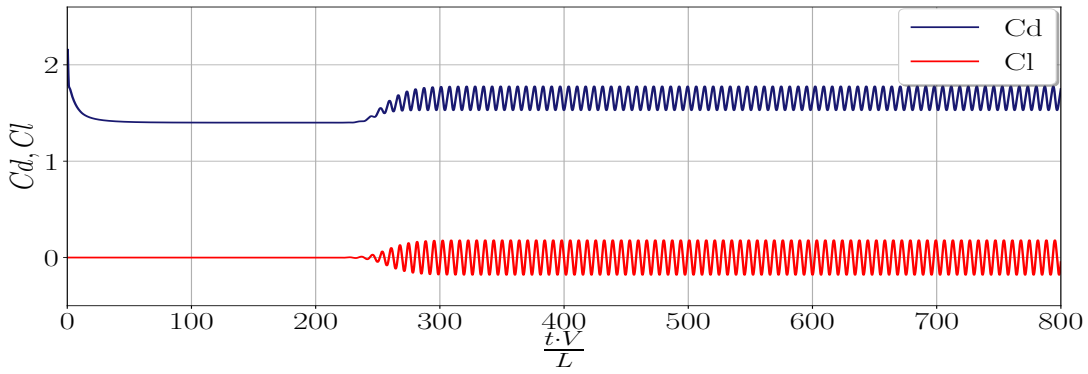

(c)

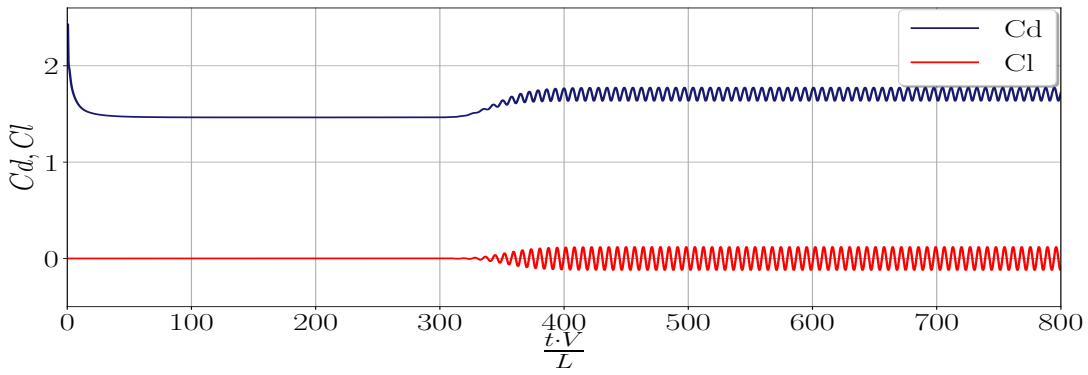

(d)

Figure 6: Drag and lift coefficients for the flow over a porous square cylinder with $Re = 10^2$: (a) $\varepsilon = 10^{-2}$, $Da = 1 \cdot 10^{-6}$, (b) $\varepsilon = 5 \cdot 10^{-2}$, $Da = 1 \cdot 10^{-5}$, (c) $\varepsilon = 10^{-1}$, $Da = 1 \cdot 10^{-4}$, (d) $\varepsilon = 1,5 \cdot 10^{-1}$, $Da = 1 \cdot 10^{-3}$.

From Fig.(4), the impact of the aforementioned parameters over the thermal energy transport can be evaluated. Higher values of porosity and permeability provide a significant improvement in thermal energy transport due to the increase of advective effects, which are more efficient than the diffusive ones. As expected, the temperature profile for the lower permeability cases are similar to those expected for a solid obstacle under the same conditions, in which the effects of thermal conduction prevail.

Table 3: Strouhal number for different values of porosity and Darcy's number.

ε	Da	St
0.01	10^{-6}	0.153744
0.05	10^{-5}	0.151212
0.10	10^{-4}	0.146217
0.15	10^{-3}	0.144945

6. CONCLUSION

The modeling of mass, energy and linear momentum transport phenomena in the laminar flow through a porous square cylinder fixed in a channel was presented. A computational model was developed and simulations were conducted aiming its validation and the solution of the flow over a heated porous structure. The analysis of the results allows the evaluation of the joint impact of porosity and permeability over the flow's characteristics.

7. ACKNOWLEDGEMENTS

The authors would like to thank PROPP-UFU, CNPq, CAPES, FAPEMIG, and Petrobras S.A. for financial and material support.

8. REFERENCES

Al-Amiri, A.M., 2000. "Analysis of momentum and energy transfer in a lid-driven cavity filled with a porous medium". *International Journal of Heat and Mass Transfer*, Vol. 43, No. 1, pp. 3513–3527.

Anirudh, K. and Dhinarakan, S., 2018. "On the onset of vortex shedding past a two-dimensional porous square cylinder". *Journal of Wind Engineering and Industrial Aerodynamics*, Vol. 179, No. 1, pp. 200–214.

Breuer, M., Bernsdorf, J., Zeiser, T. and Durst, F., 2000. "Accurate computations of the laminar flow past a square cylinder based on two different methods: lattice-boltzmann and finite-volume". *International Journal of Heat and Fluid Flow*, Vol. 21, No. 1, pp. 186–196.

Chen, X., Winoto, S.H., Yu, P. and Low, H.T., 2008. "Numerical analysis for the flow past a porous square cylinder based on the stress-jump interfacial-conditions". *International Journal of Numerical Methods for Heat and Fluid Flow*, Vol. 18, No. 5, pp. 635–655.

Dhinakaran, S. and Ponmozhi, J., 2011. "Heat transfer from a permeable square cylinder to a flowing fluid". *Energy Conversion and Management*, Vol. 52, No. 1, pp. 2170–2182.

Goyeau, B. and Songbe, J.P., 1996. "Numerical study of double-diffusive natural convection in a porous cavity using the darcy-brinkman formulation". *International Journal of Heat and Mass Transfer*, Vol. 39, No. 7, pp. 1363–1378.

Lauriat, G. and Prasad, V., 1989. "Non-darcian effects on natural convection in a vertical porous enclosure". *International Journal of Heat and Mass Transfer*, Vol. 32, No. 11, pp. 2135–2148.

Mahdhaoui, H., Chesneau, X. and Laatar, A.H., 2017. "Numerical simulation of flow through a porous square cylinder". *Energy Procedia*, Vol. 139, No. 1, pp. 785–790.

Robichaux, J., Balachandar, S. and Vanka, S.P., 1999. "Three-dimensional floquet instability of the wake of square cylinder". *Physics of Fluids*, Vol. 11, No. 1, pp. 560–578.

Sahu, A.K., Chhabra, R.P. and Eswaran, V., 2009. "Two-dimensional unsteady laminar flow of a power law fluid across a square cylinder". *Journal of Non-Newtonian Fluid Mechanics*, Vol. 160, No. 1, pp. 157–167.

Sharma, A. and Eswaran, V., 2004. "Heat and fluid flow across a square cylinder in the two-dimensional laminar flow regime". *Numerical Heat Transfer*, Vol. 45, No. 1, pp. 247–269.

Vafai, K., 2005. *Handbook of Porous Media*. Taylor & Francis Group, 6000 Broken Sound Parkway NW, Suite 300, 2nd edition.

9. RESPONSIBILITY NOTICE

The authors are the only responsible for the printed material included in this paper.